NASA TECHNICAL MEMORANDUM

NASA TM X-983

NASA TM X-983

EXPERIMENTAL DATA ON STAGNATION-POINT GAS INJECTION COOLING ON A HEMISPHERE-CONE IN A HYPERSONIC ARC TUNNEL

by John E. Grimaud and Leonard C. McRee

Langley Research Center
Langley Station, Hampton, Va.

NATIONAL AERONAUTICS AND SPACE ADMINISTRATION • WASHINGTON, D. C. • JULY 1964

EXPERIMENTAL DATA ON STAGNATION-POINT GAS INJECTION COOLING ON A HEMISPHERE-CONE IN A HYPERSONIC ARC TUNNEL

By John E. Grimaud and Leonard C. McRee

Langley Research Center
Langley Station, Hampton, Va.

NATIONAL AERONAUTICS AND SPACE ADMINISTRATION

For sale by the Office of Technical Services, Department of Commerce,
Washington, D.C. 20230 -- Price $0.75

EXPERIMENTAL DATA ON STAGNATION-POINT GAS INJECTION COOLING ON A HEMISPHERE-CONE IN A HYPERSONIC ARC TUNNEL

By John E. Grimaud and Leonard C. McRee
Langley Research Center

SUMMARY

25789

Exploratory tests were made to determine the reduction of heat transfer resulting from ejection of gases at the stagnation point on a hemisphere-cone at a nominal Mach number of about 9 and at stagnation enthalpies up to 1600 Btu/lb. Helium, nitrogen, and argon gases were used as coolants. The ratio of mass flow of coolant to the mass flow of air swept out by the model projected area was less than 0.20 in all cases.

The experimental heat-transfer data were normalized by the calculated stagnation-point values based on test conditions in the tunnel and are presented as a function of the surface distance from the stagnation point. The variation of shock standoff distances with mass flow and volumetric flow of the gaseous ejectants is presented along with photographs of the luminous flow field of the model during tests.

Author

INTRODUCTION

Cooling by a fluid injection is a form of mass transfer cooling which appears promising as a mechanism for heat absorption and blockage during hypersonic reentry. (For example, see ref. 1.) In addition, the technique appears adaptable for use as a possible solution to the communication blackout problem during reentry. In this case high rates of fluid injection could be used for short periods of time in the vicinity of an antenna in an attempt to quench the ionized flow near the antenna. A number of theoretical analyses have been made in order to attempt to predict the cooling effectiveness of mass transfer cooling (for example, refs. 1 to 5); however, only a limited number of experimental investigations pertaining to fluid injection have been conducted. (Refs. 6 to 9 are typical.) In addition to the sparsity of experimental work, a further hindrance to the advancement of the current status of the problem lies in the fact that the bulk of the investigations were made in cold flow facilities. At present, little is known concerning the applicability of these data to a body in a hot environment.

The present tests were made in the 900-kilowatt continuous-arc tunnel at the Langley Research Center (ref. 10), which has been subsequently modified to higher power, pressure, and Mach number. The purpose of the test program, which was exploratory in nature, was to measure heat transfer and shock stand-off distances on a hemisphere-cone with gaseous ejection cooling at the stagnation point. The model was tested at a nominal Mach number of 9 and at stagnation enthalpies up to 1600 Btu/lb. Helium, nitrogen, and argon were used as coolants.

This report includes an appendix by Roger B. Stewart of the Langley Research Center, which presents a discussion of the stagnation enthalpy determination by a sonic throat analysis.

SYMBOLS

A	area, sq ft
c_p	specific heat at constant pressure, Btu/lb-^{o}R
c_v	specific heat at constant volume, Btu/lb-^{o}R
d	throat diameter, in.
h	enthalpy, Btu/lb
M	Mach number
$\dot{m}$	mass flow, lb/sec
p	pressure, lb/sq ft
q	heat-transfer rate, Btu/(sq ft)(sec)
R	gas constant, 6.855×10^{-2} Btu/lb-^{o}R
r	nose radius, in.
s	distance along body from stagnation point of hemisphere, in.
T	temperature, ^{o}R
t	model-wall thickness, in.
u	velocity, ft/sec

V	volumetric flow, cu ft/sec
x	shock standoff distance, in.
γ	ratio of specific heats, c_p/c_v
ρ	density, lb/cu ft
τ	time, sec

Subscripts:

a	air
c	coolant
cold	tunnel operating with arc off
hot	tunnel operating with arc on
l	local
o	reference conditions (see table I)
s	stagnation-point value
t	total
w	wall
∞	free-stream conditions
1	conditions before shock
2	conditions after shock

Superscript:

*	sonic throat

EQUIPMENT AND PROCEDURE

Tunnel

The investigation was conducted in the 900-kilowatt continuous-arc tunnel at the Langley Research Center and is described in reference 10. A schematic illustration and a photograph showing the appearance of the tunnel are presented

in figure 1. The facility consisted of an arc heater, arc chamber, plenum chamber, throat section, a 5° half-angle conical nozzle, a 3-inch-diameter cylindrical test section, a straight pipe diffuser, and a steam ejector. Test air was supplied to the arc chamber from a storage tank at a pressure of 500 lb/sq in. The high-pressure air system was also used to pressurize the water storage bottles which furnished cooling water to the different components of the tunnel. Typical flow conditions in the tunnel can be seen in table I.

A 16-millimeter motion-picture camera was used to make a visual record of each test. These movies were used to provide qualitative information of the flow field, to determine the time of model injection into the stream, and for measurements of the variation in the shock standoff distance with coolant injections.

Models

For this investigation, a hemisphere-cone-cylinder configuration was selected (fig. 2). The model had a nose radius of 0.145 inch, a conical forebody angle of 9°, and a cylindrical section diameter of 0.500 inch. The length of the model was 3.797 inches. The 347 stainless-steel model was hollow and had thin walls. The nominal wall thickness was 0.020 inch at the thermocouple stations.

Two models of the configuration were made. One model was used to measure heat transfer during the tests with no-coolant flow, and the instrumentation (thermocouples) for this model is shown in figure 2. The other model was used to measure heat transfer during the coolant-injection tests. This model had an internal coolant-flow tube of 0.040-inch inside diameter which exited at the stagnation point of the model. The thermocouple locations on this model were identical to the no-coolant-flow model, with the exception of the one at the stagnation point.

All thermocouples were of No. 30 chromel-alumel wire. The thermocouple wires were extended through holes drilled in the model surface, twisted together, and silver soldered. The wires were then smoothed and made flush with the model surface. The thickness of the model surface at the thermocouple locations was measured on the test models.

Tests and Test Procedure

The tunnel flow conditions for each test are presented in table I. Also included in the table are the types of coolants used, coolant-injection coefficients, and the theoretical stagnation-point heat-transfer rates.

The data were obtained from tests of two types. First, one model of the configuration with no-coolant injection was used to measure heat-transfer rates. (See fig. 2.) Secondly, the model with coolant ejecting through a tube at the stagnation point was used to determine the heat transfer in the presence of coolant injection. A typical test sequence was as follows: (a) the mass flow of the coolant was set, (b) the arc was ignited and tunnel flow conditions were

established, and (c) the room-temperature, isothermal model was injected into the stream. The gaseous coolants were approximately at room temperature. The injection apparatus with the test model mounted on it can be seen in figure 3. The apparatus was mounted in the tunnel-window cavity and this apparatus injected the model into test position (at zero angle of attack) in approximately 0.05 second. The rapid injection of the model into the airstream insured a step-function exposure to tunnel flow conditions. The average length of time that the model remained in the stream was 3 seconds. During this time the millivolt outputs of the thermocouples located on the model surface were recorded on a multichannel oscillograph as continuous traces representing temperature at any given time. The thermocouple junction box temperature was at ambient temperature and was recorded before each run.

The gaseous coolants ejected at the stagnation point of the model were helium, nitrogen, and argon. The coolants were obtained from commercial bottles, passed through a pressure regulator, and then through a tube-and-ball-float flowmeter. The metering pressure was kept constant at 25 lb/sq in. while the flowmeter size was varied to give injection coefficient values that ranged from 0 to 0.20. (See eq. (3).)

Data Reduction

The technique used for determining the enthalpy in this investigation was the commonly designated "sonic-throat" method. The stagnation enthalpy using the sonic-flow technique was obtained from the following equation for the static enthalpy at the nozzle throat:

$$h^* = 0.0312\left(T_{t,1_{cold}}\right)^{1.25}\left(\frac{p_{t,1_{hot}}}{p_{t,1_{cold}}}\frac{\dot{m}_{cold}}{\dot{m}_{hot}}\right)^{2.5} \qquad (1)$$

and the Mollier diagram for equilibrium air. The development of equation (1) is given in the appendix to this report.

In equation (1), $T_{t,1}$ is the inlet temperature of the air to the tunnel, $p_{t,1}$ is the stagnation pressure in the arc chamber, and $\dot{m}$ is the measured mass flow.

Free-stream conditions and conditions behind the model bow shock were calculated from the continuity, momentum, and energy equation (ref. 11) and the Mollier diagram for equilibrium air (ref. 12) assuming a one-dimensional isentropic equilibrium expansion down the nozzle. Mach numbers were obtained from pitot pressure measurements.

The heat-transfer data were reduced on the assumption that heat losses due to radiation and lateral conduction were negligible. With these assumptions, the local heat transfer is determined by using the one-dimensional transient heat-flow equation:

$$q = \rho c_p t \frac{dT_w}{d\tau} \tag{2}$$

To find the time rate of change of temperature $dT_w/d\tau$, the slope of the temperature-time curve was taken at a small time after injection into the stream when it was judged that the initial transients had disappeared. At this time the enthalpy potential and heat-transfer rates across the boundary layer were a maximum because the model was still near ambient temperature. The specific heat c_p was assumed constant at 0.11 Btu/lb-^{o}R and independent of temperature for the range of temperatures for which the data were evaluated. The value of the density ρ for 347 stainless steel was taken to be 493.5 lb/cu ft, and the thickness t was the measured wall thickness at each thermocouple location. The dimensionless heat-transfer parameter q_l/q_s was defined as the ratio of measured local heat-transfer rate to the theoretical heat-transfer rate at the stagnation point calculated from reference 13. It was necessary to present the results in the dimensionless manner in order to account for the variations in enthalpy that existed in the tunnel for different tests.

The coolant injection rate was expressed as the parameter $\dot{m}_c/\dot{m}_a$, which is defined as the ratio of coolant mass injection rate to the mass rate of air swept out by the projected frontal area of the model:

$$\frac{\dot{m}_c}{\dot{m}_a} = \frac{\dot{m}_c}{\rho_\infty u_\infty A} \tag{3}$$

This parameter is based on calculated free-stream properties, and the dimensionless heat transfer and shock standoff distance are presented as a function of this parameter.

In figure 4, typical photographs of the model undergoing tests (obtained from the 16-millimeter motion pictures) are shown. Although most of the reproductions shown here lack clarity, the original film records revealed more details of the flow phenomenon.

Accuracy

The estimated accuracies of the model and test parameters are given below:

Mach number	±0.1
Wall thickness of model at thermocouple stations, in.	±0.002
Stagnation enthalpy, Btu/lb	±100
Stagnation pressure, lb/sq in.	±4

RESULTS AND DISCUSSION

Shock Standoff Distance

Shock standoff distances measured from the film records of the test are shown in figures 5 and 6 plotted, respectively, against mass injection coefficient and volumetric injection ratio for the different coolants used. In the measurements of these distances it was assumed that the upstream edge of the luminous gas cap and the upstream edge of the bow shock were coincident. Further, in order to check for oscillatory movements of the shock, several frames from the film records of one test were measured. Results from these measurements, made on an optical comparator, showed consistent agreement. In figure 5, the dependence of the shock standoff distance on type of coolant and coolant injection rate is clearly shown. For the same mass injection rate, it is seen that a greater shock standoff distance is produced by the lighter gas helium, as compared to the heavier gases nitrogen and argon. On the other hand, the heavier gases produced the greater standoff distance for the same volumetric flow (fig. 6) as compared to that of the light gas helium. (Note that the curve for helium contains data from an auxiliary model which had a nose radius of 0.109 inch.) Although the shock standoff distance could not be accurately obtained for zero injection in this investigation, good agreement is shown when the experimental curves of figures 5 and 6 for finite injection rates are faired in with a theoretical shock standoff distance taken from reference 14. These data showing the variation of shock standoff distance with coolant flow apply only for the geometry used in this investigation. Results presented in reference 15 show that such things as the ratio of model to jet diameter, the jet Mach number, and the free-stream Mach number can influence the shock standoff distance and in some cases alter the bow shock shape.

Heat Transfer

The heat-transfer data obtained on the model are presented in figures 7 and 8 for the three coolant gases employed in the investigation. The heat-transfer parameter q_l/q_s used in the figures is the ratio of the measured local heat-transfer rate to the stagnation-point heat-transfer rate calculated from reference 13. The dashed curve shown in figure 7 gives the theoretical dimensionless heat-transfer distribution along the hemisphere-cone surface for the no-coolant-flow case. The heat-transfer data obtained from the stagnation-point thermocouple appeared to be significantly affected by conduction effects, and are not shown in figure 7. The heat-transfer rates measured on the conical surface of the model (by the thermocouples located at $s/r = 2.999$ and $s/r = 3.8965$) are believed to be free of significant conduction effects as evidenced by the reasonable agreement between theory and experiment at this location for the no-coolant-flow case. (See fig. 7.) For the maximum coolant injection rates of these tests a reduction to one-third or less in the value of q_l/q_s is achieved with the different coolants. It is indicated in figure 7 that for the lower coolant injection rates, the body heating rates initially tend to increase with coolant injection. This phenomenon has been observed in similar tests at lower enthalpy (cold, supersonic tests, ref. 7).

Examination of figure 8 (a cross plot of fig. 7) at the higher injection coefficients indicates that for s/r values of less than 4, considerably larger mass flows of nitrogen or argon are required for a given reduction of heating rate than was needed for helium.

Langley Research Center,
National Aeronautics and Space Administration,
Langley Station, Hampton, Va., February 12, 1964.

APPENDIX

STAGNATION ENTHALPHY DETERMINATION BY A SONIC THROAT ANALYSIS

By Roger B. Stewart

The following development leads to an expression for the static enthalpy at a sonic throat. This expression was previously used in specifications on an arc heater prepared at the Ames Research Center, but as far as is known, a discussion of the development and usefulness of the equation has not yet been published.

Flow properties have been obtained in references 16 and 17 for the isentropic, equilibrium expansion of high-temperature air. With a knowledge of two properties at sonic conditions the other properties are uniquely specified and a plot of $\frac{\rho^* A^* u^*}{p_t A^*}$ as a function of h_t can be made (chart 14 of ref. 17). In a similar fashion, a slightly different plot can be made of $\log \frac{p_t A^*}{\dot{m}}$ as a function of $\log h^*$. Such a plot is shown in figure 9.

For the stagnation enthalpy range of about $500 \leqq h_t \leqq 8000$ Btu/lb, a straight line fit will give fair agreement to computed data. If the intercept is taken at $\log h^* = 0$, the following equation of the form $y = mx + b$ can be written:

$$\log \frac{p_t A^*}{\rho^* A^* u^*} = 0.4 \log h^* + 0.876 \tag{A1}$$

or

$$\log h^* = 2.5 \log \frac{p_t A^*}{\rho^* A^* u^*} - 2.5 \log 7.52$$

$$= \log 0.00645 \left(\frac{p_t A^*}{\dot{m}} \right)^{2.5} \tag{A2}$$

so that

$$h^* = 0.00645 \left(\frac{p_t A^*}{\dot{m}} \right)^{2.5} \tag{A3}$$

For a cold perfect gas with $\gamma = 1.4$, $\frac{\rho^* A^* u^*}{p_t A^*} T_t^{1/2}$ is constant, and

$$\left[\frac{\dot{m}_{cold}\left(T_{t,cold}\right)^{1/2}}{p_{t,cold} A^*_{cold}}\right]^{2.5} = 0.207 \qquad (A4)$$

Equation (A3) can be multiplied by

$$\left[\frac{\dot{m}_{cold}\left(T_{t,cold}\right)^{1/2}}{p_{t,cold} A^*_{cold}}\right]^{2.5} \frac{1}{0.207}$$

without changing its value and rewritten as:

$$h^* = 0.0312\left(T_{t,cold}\right)^{1.25}\left(\frac{\dot{m}_{cold}}{p_{t,cold} A^*_{cold}} \frac{p_{t,hot} A^*_{hot}}{\dot{m}_{hot}}\right)^{2.5} \qquad (A5)$$

The sole purpose for introducing the cold-perfect-gas quantities is that equation (A3) demands a knowledge of the effective hot-throat area, A^*_{hot}, and for the small throat used in the investigation of this report (0.133 inch) it seemed unlikely that the effective throat area would be the same as the geometric throat area. Note that h^* and thus h_t are functions of $(d^*)^{5.0}$ which makes a knowledge of the effective throat size a critical factor. If it is assumed that $\frac{A^*_{hot}}{A^*_{cold}} = 1$, then the problem of obtaining A^*_{hot} can be avoided by use of equation (A5). In some recent work reported in reference 18, the results showed that for the particular tunnel geometry tested, the effective throat area appeared to be equal to the geometric throat area. This was not the case for the tunnel geometry used in the present investigation. A recent study made with the arc heater exhausting through the sonic throat into a water-cooled, total calorimeter has shown that for the tunnel geometry used in the present investigation (and also for several different throat sizes), the effective throat area is not equal to the geometric area. Assuming that they are equal produces an error in stagnation enthalpy determination as high as a factor of 2. On the other hand, using equation (A5) and by a careful control of the throat Reynolds number between cold and hot running conditions, it should be possible to obtain a ratio of $\frac{A^*_{hot}}{A^*_{cold}}$ very close to unity so that this equation would yield valid results. Because the throat Reynolds number decreases when the arc is struck, it is necessary to operate under cold running conditions with a sufficiently low stagnation pressure so that a minimum change

occurs between the cold and hot throat Reynolds numbers. For the magnetically stabilized arc heater of this investigation, this control was accomplished by operating with the cold stagnation pressure held to a relatively low value, $p_{t,cold} \leqq 110$ lb/sq in. abs.

REFERENCES

1. Roberts, Leonard: Mass Transfer Cooling Near the Stagnation Point. NASA TR R-8, 1959. (Supersedes NACA TN 4391.)

2. Swenson, Bryon L.: An Approximate Analysis of Film Cooling on Blunt Bodies by Gas Injection Near the Stagnation Point. NASA TN D-861, 1961.

3. Libby, Paul A.: The Homogeneous Boundary Layer at an Axisymmetric Stagnation Point With Large Rates of Injection. WADD Tech. Rep. 60-435, U.S. Air Force, Dec. 1960.

4. Chung, Paul M.: Effect of Localized Mass Transfer Near the Stagnation Region of Blunt Bodies in Hypersonic Flight. NASA TN D-141, 1960.

5. Reshotko, Eli, and Cohen, Clarence B.: Heat Transfer at the Forward Stagnation Point of Blunt Bodies. NACA TN D-3513, 1955.

6. Warren, C. Hugh E.: An Experimental Investigation of the Effect of Ejecting a Coolant Gas at the Nose of a Blunt Body. GALCIT Memo. No. 47 (Contract No. DA-04-495-Ord-19), Dec. 15, 1958.

7. Stalder, Jackson R., and Inouye, Mamoru: A Method of Reducing Heat Transfer to Blunt Bodies by Air Injection. NACA RM A56B27a, 1956.

8. Dannenberg, Robert E.: Helium Film Cooling on a Hemisphere at a Mach Number of 10. NASA TN D-1550, 1962.

9. Libby, Paul A., and Cresci, Robert J.: Experimental Investigation of the Downstream Influence of Stagnation-Point Mass Transfer. Jour. Aerospace Sci., vol. 28, no. 1, Jan. 1961, pp. 51-64.

10. Boatright, William B., Stewart, Roger B., and Grimaud, John E.: Description and Preliminary Calibration Tests of a Small Arc-Heated Hypersonic Wind Tunnel. NASA TN D-1377, 1962.

11. Ames Research Staff: Equations, Tables, and Charts for Compressible Flow. NACA Rep. 1135, 1953. (Supersedes NACA TN D-1428.)

12. Feldman, Saul: Hypersonic Gas Dynamic Charts for Equilibrium Air. Res. Rep. 40, Avco-Everett Res. Lab., Jan. 1957.

13. Lees, Lester: Laminar Heat Transfer Over Blunt-Nosed Bodies at Hypersonic Flight Speeds. Jet Propulsion, vol. 26, no. 4, Apr. 1956, pp. 259-269, 274.

14. Hayes, Wallace D., and Probstein, Ronald F.: Hypersonic Flow Theory. Academic Press, Inc. (New York), 1959.

15. Romeo, David J., and Sterrett, James R.: Exploratory Investigation of the Effect of a Forward-Facing Jet on the Bow Shock of a Blunt Body in a Mach Number 6 Free Stream. NASA TN D-1605, 1963.

16. Yoshikawa, Kenneth K., and Katzen, Elliott D.: Charts for Air-Flow Properties in Equilibrium and Frozen Flows in Hypervelocity Nozzles. NASA TN D-693, 1961.

17. Jorgensen, Leland H., and Baum, Gayle M.: Charts for Equilibrium Flow Properties of Air in Hypervelocity Nozzles. NASA TN D-1333, 1962.

18. Arney, G. D., Jr., and Boylan, D. E.: A Calorimetric Investigation of Some Problems Associated With a Low-Density Hypervelocity Wind Tunnel. AEDC-TDR-63-19 (Contract No. AF40(600)-1000), Arnold Eng. Dev. Center, Feb. 1963.

TABLE I.- TEST CONDITIONS

$\left[T_o = 491.42^o \text{ R};\ \rho_o = 0.080722 \text{ lb/cu ft};\ RT_o = 33.68 \text{ Btu/lb}\right]$

Test	$p_{t,1}$, atm	$T_{t,1}$, ^oR	$\frac{h_{t,1}}{RT_o}$	M_1	$\frac{\rho_1}{\rho_o}$	$p_{t,2}$, atm	Coolant	$\frac{\dot{m}_c}{\dot{m}_a}$	q_s, Btu/(sq ft)(sec)
1	17.55	4012	32.98	9.2	11.4×10^{-4}	0.06669	None	----------	290.52
2	20.07	5475	48.92	8.4	8.8	.07626	None	----------	422.03
3	18.90	4874	41.82	8.8	9.7	.07212	Helium	6.250×10^{-2}	423.77
4	19.32	5190	45.42	8.6	9.3	.07345	Helium	1.891	434.03
5	19.32	4410	36.90	9.0	11.2	.07345	Helium	2.748	346.71
6	20.07	3905	31.94	9.1	13.8	.07626	Helium	.846	301.14
7	18.43	3780	30.71	9.2	13.0	.07005	Helium	.186	283.57
8	19.12	4690	39.81	8.9	10.4	.07264	Nitrogen	7.290	375.84
9	17.96	4025	33.06	9.0	11.5	.06824	Nitrogen	.598	270.32
10	18.64	4470	37.49	8.9	10.6	.07083	Nitrogen	16.052	334.82
11	19.52	5310	42.72	8.9	9.9	.07419	Nitrogen	2.635	437.69
12	19.52	4830	41.32	9.0	10.3	.07419	Argon	20.486	428.49
13	18.64	4400	36.78	9.0	10.8	.07083	Argon	4.633	336.93
14	19.86	4900	42.12	8.9	10.0	.07548	Argon	1.270	439.39
15	19.30	5050	43.72	8.7	9.2	.07334	Argon	10.084	422.46
16	20.40	5100	43.93	8.7	10.0	.07755	Argon	4.695	434.64

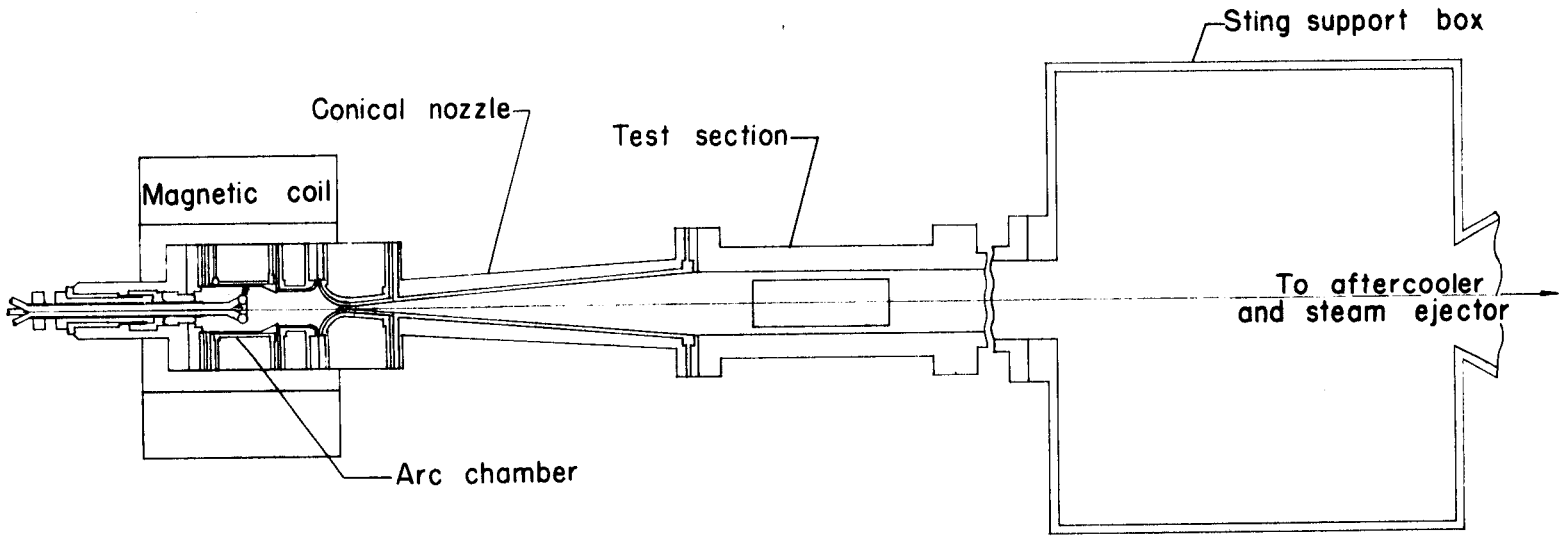

(a) Schematic illustration.

Figure 1.- Schematic illustration and photograph of the 900-kilowatt continuous-arc tunnel.

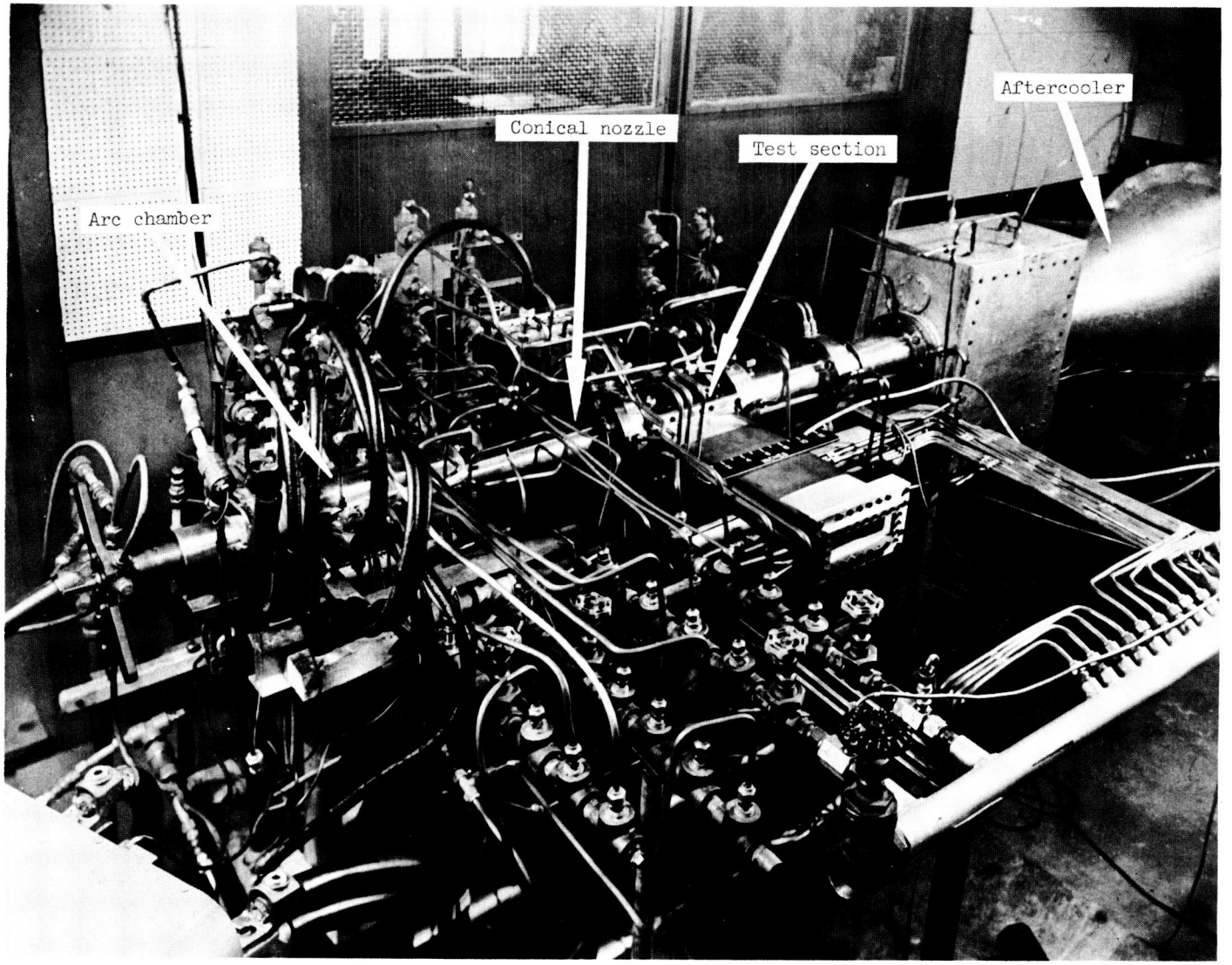

(b) Photograph. L-60-7288

Figure 1.- Concluded.

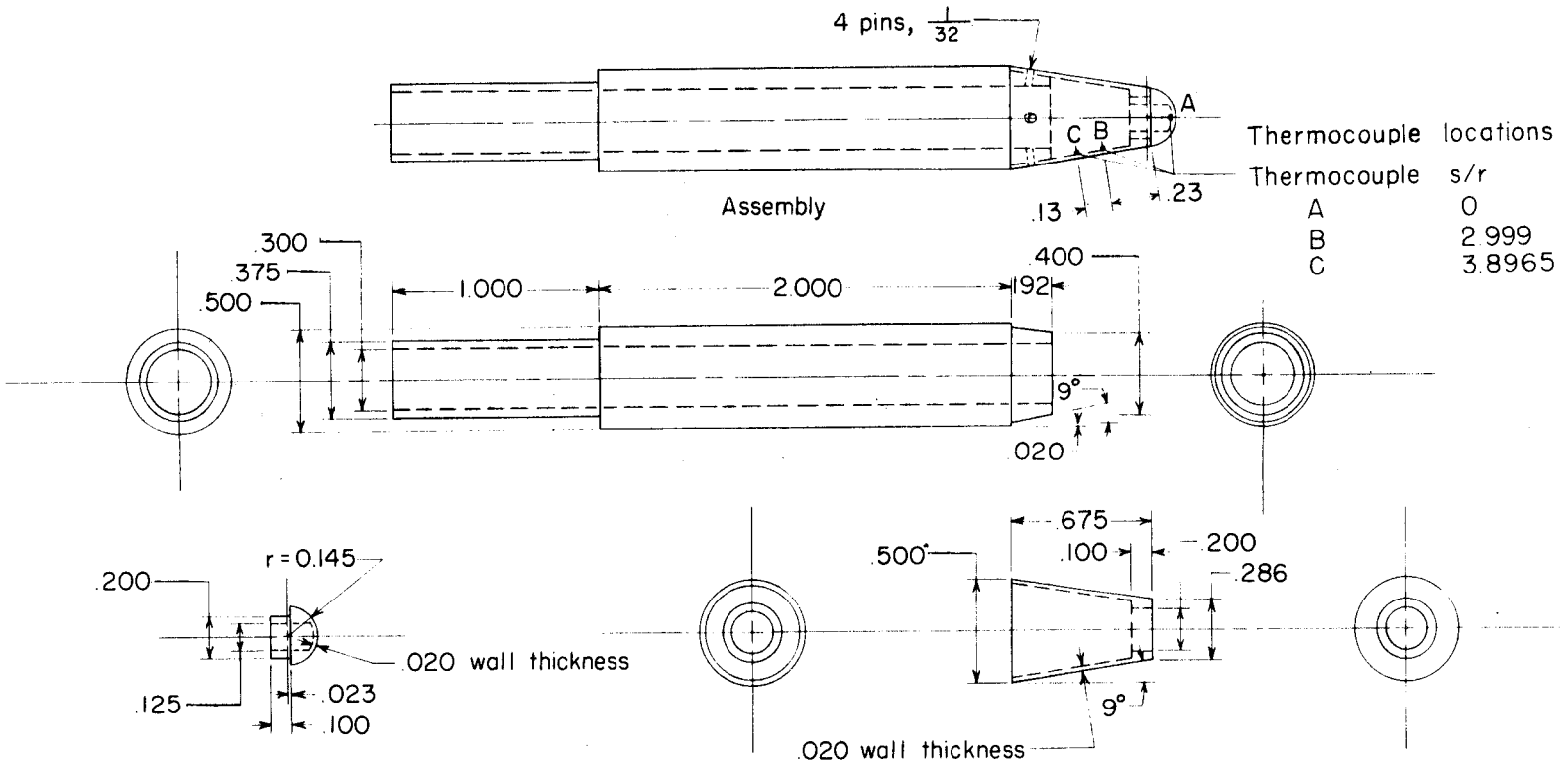

Figure 2.- Detailed drawing of model. All dimensions are in inches.

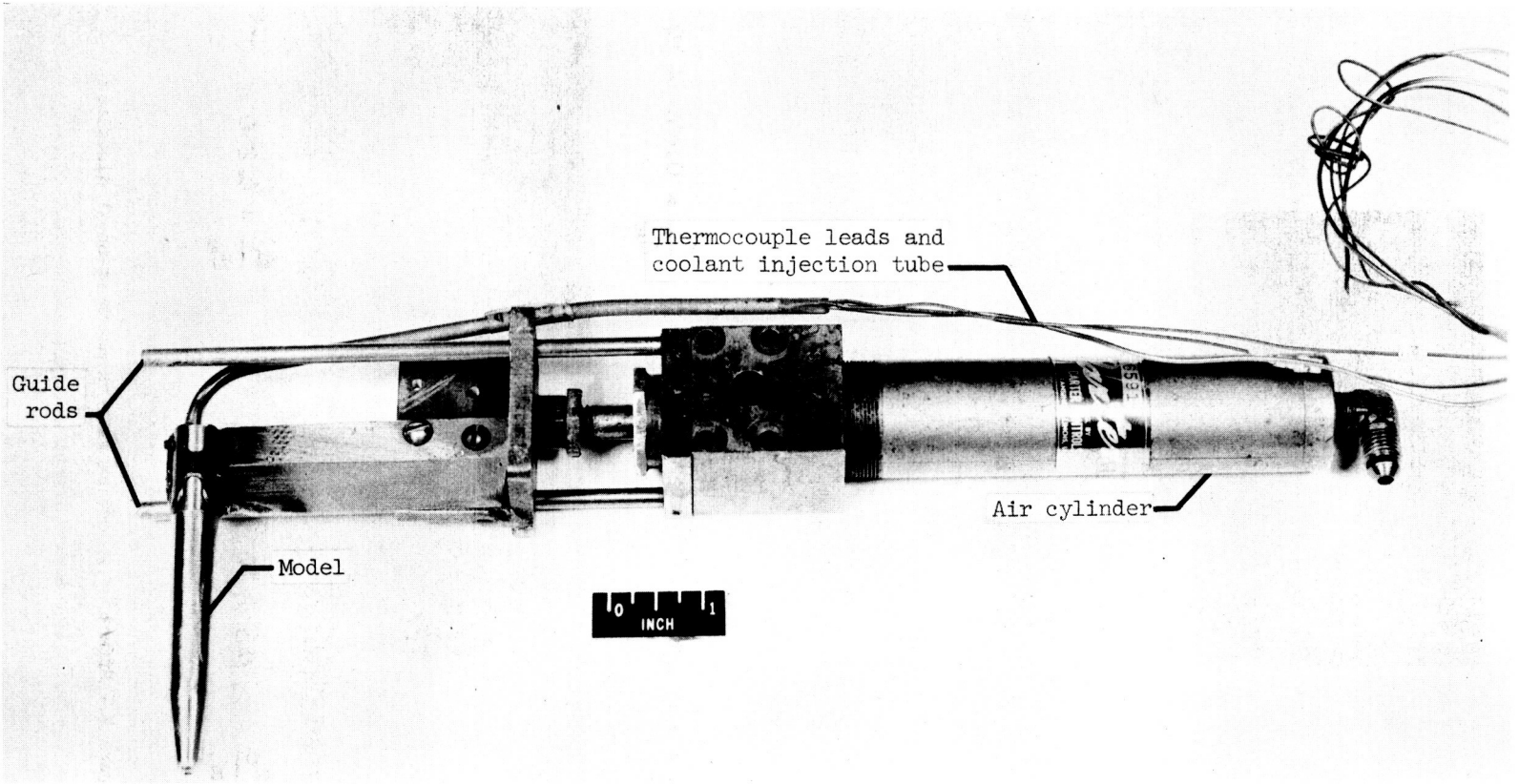

Figure 3.- Model mounted to injection apparatus in retracted position. L-62-8082.1

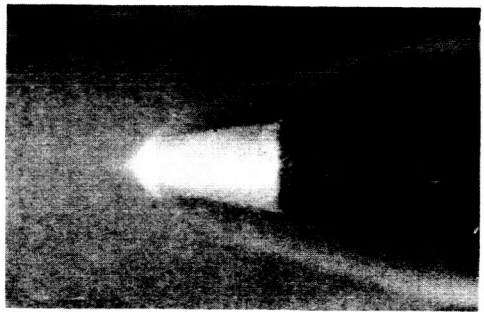

$\frac{\dot{m}_c}{\dot{m}_a} = 0$

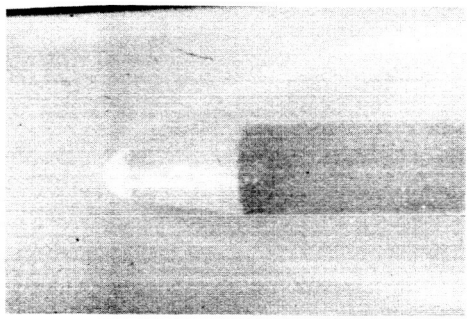

$\frac{\dot{m}_c}{\dot{m}_a} = 0.186 \times 10^{-2}$

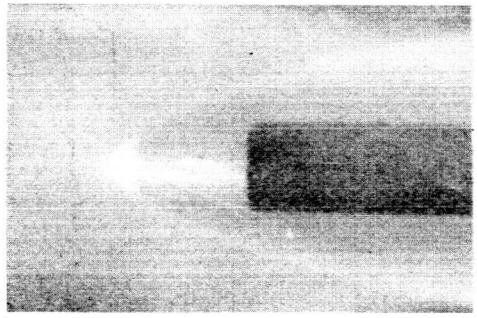

$\frac{\dot{m}_c}{\dot{m}_a} = 0.846 \times 10^{-2}$

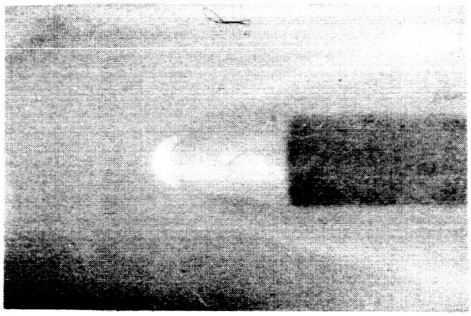

$\frac{\dot{m}_c}{\dot{m}_a} = 2.748 \times 10^{-2}$

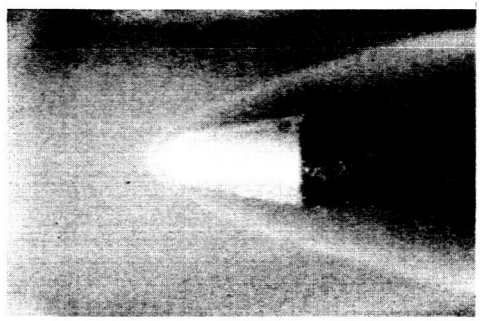

$\frac{\dot{m}_c}{\dot{m}_a} = 6.250 \times 10^{-2}$

(a) Helium.

Figure 4.- Effect of injection rate on shock standoff distance. L-64-415

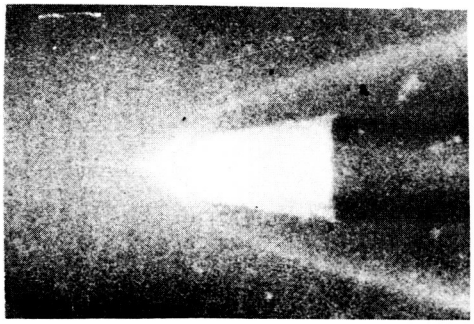

$\frac{\dot{m}_c}{\dot{m}_a} = 0$

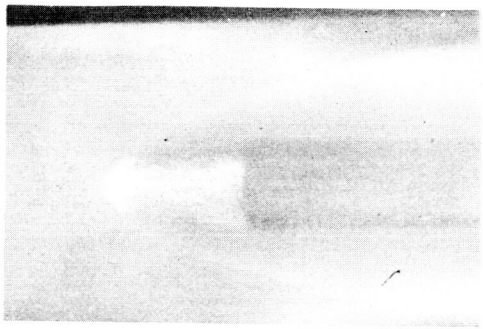

$\frac{\dot{m}_c}{\dot{m}_a} = 0.598 \times 10^{-2}$

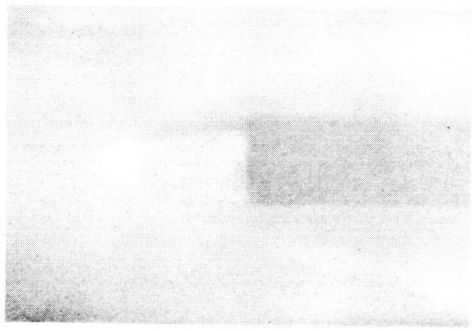

$\frac{\dot{m}_c}{\dot{m}_a} = 2.635 \times 10^{-2}$

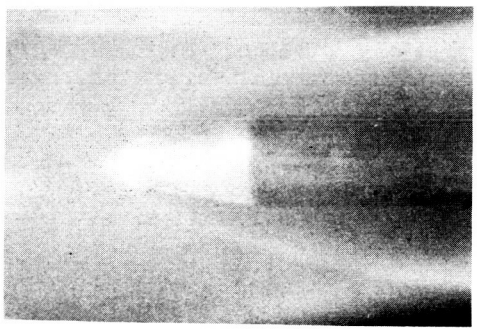

$\frac{\dot{m}_c}{\dot{m}_a} = 7.290 \times 10^{-2}$

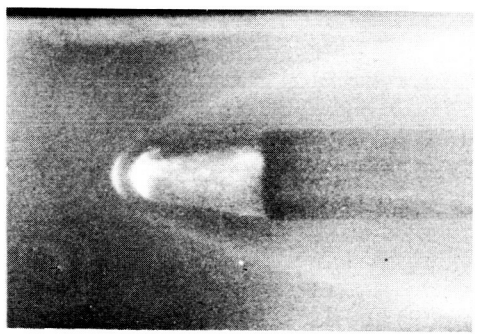

$\frac{\dot{m}_c}{\dot{m}_a} = 16.052 \times 10^{-2}$

(b) Nitrogen.

Figure 4.- Continued.

L-64-416

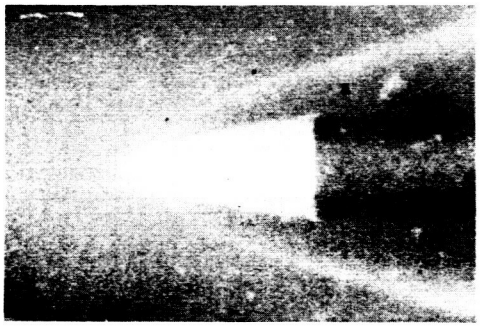

$\frac{\dot{m}_c}{\dot{m}_a} = 0$

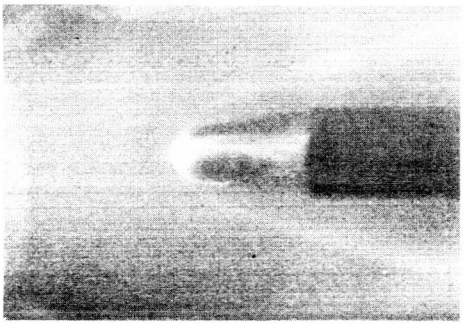

$\frac{\dot{m}_c}{\dot{m}_a} = 1.270 \times 10^{-2}$

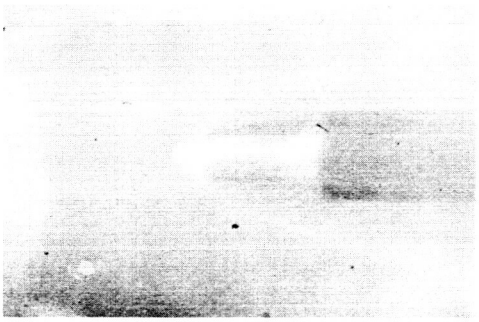

$\frac{\dot{m}_c}{\dot{m}_a} = 4.633 \times 10^{-2}$

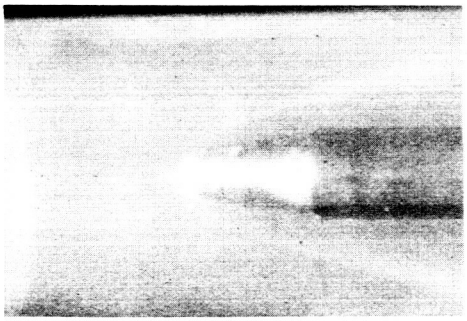

$\frac{\dot{m}_c}{\dot{m}_a} = 4.695 \times 10^{-2}$

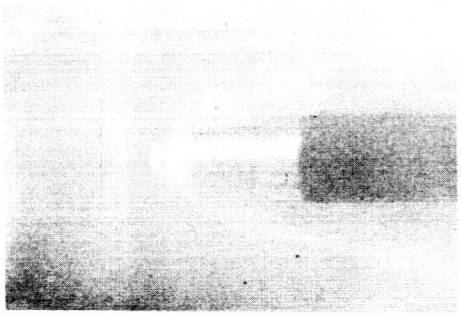

$\frac{\dot{m}_c}{\dot{m}_a} = 10.084 \times 10^{-2}$

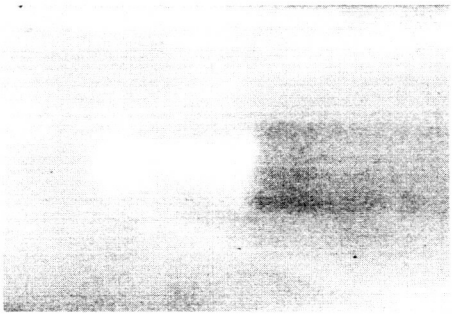

$\frac{\dot{m}_c}{\dot{m}_a} = 20.486 \times 10^{-2}$

(c) Argon.

Figure 4.- Concluded. L-64-417

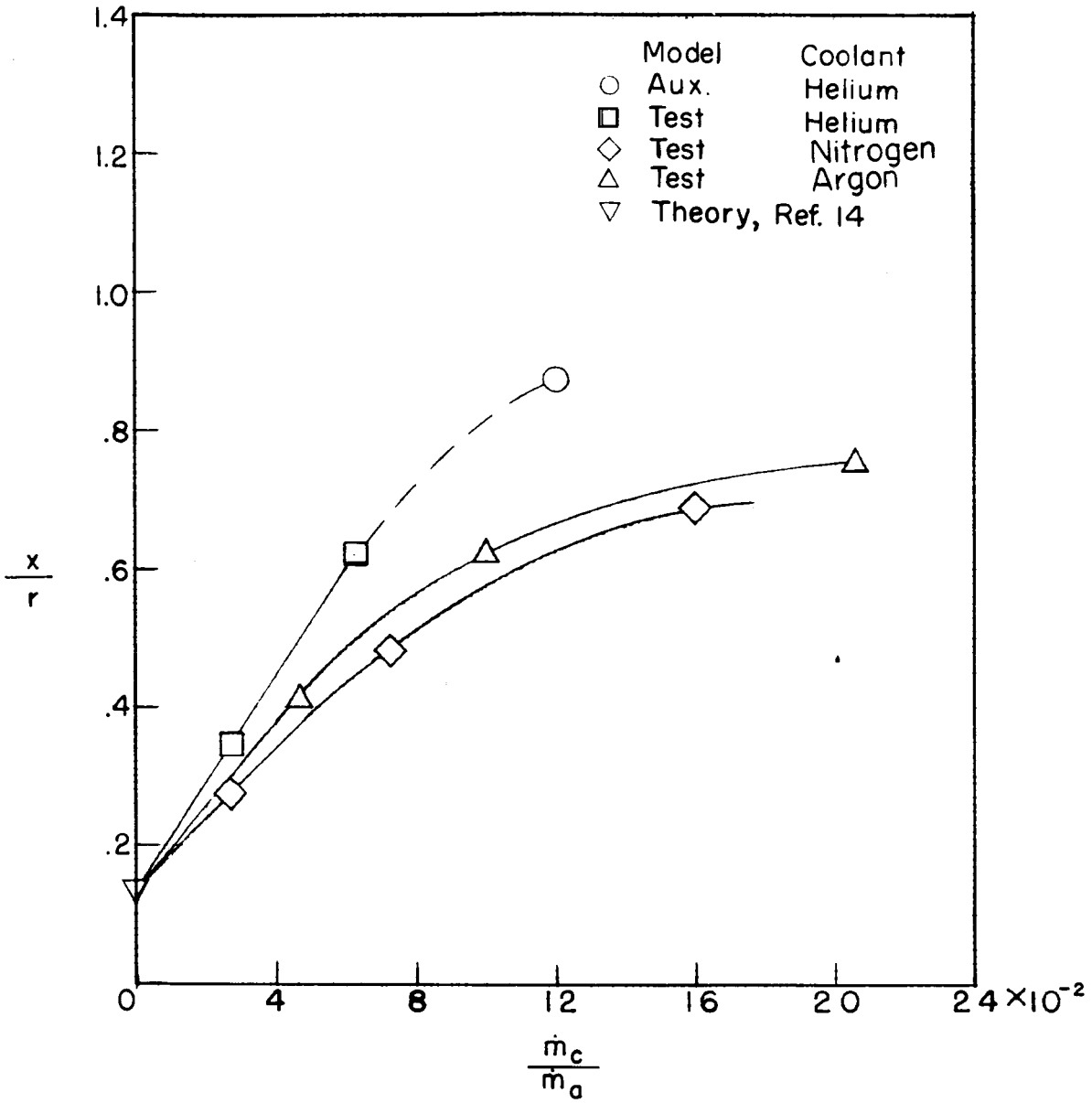

Figure 5.- Shock standoff as a function of mass injection.

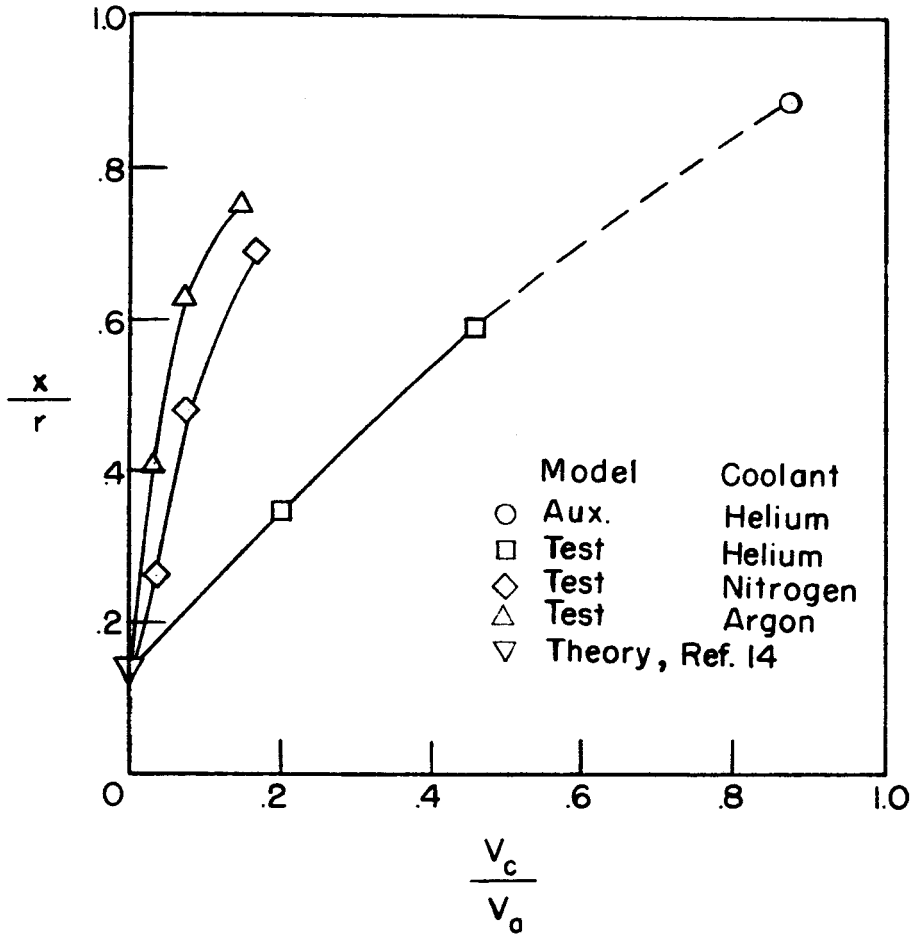

Figure 6.- Shock standoff as a function of volumetric flow.

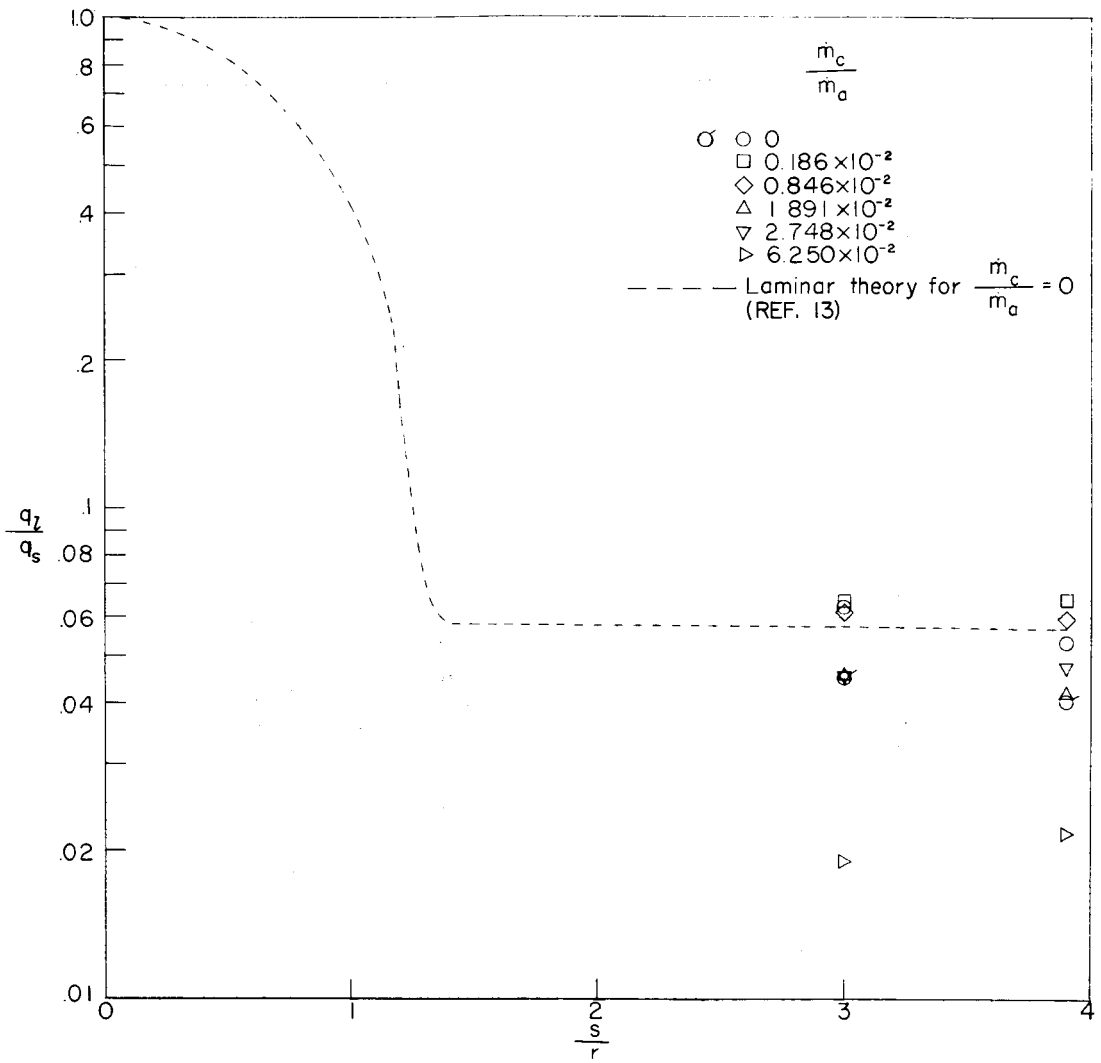

(a) Helium coolant.

Figure 7.- Variation of heating rate with coolant injection. Laminar theory obtained from reference 13. Flagged symbols denote check points.

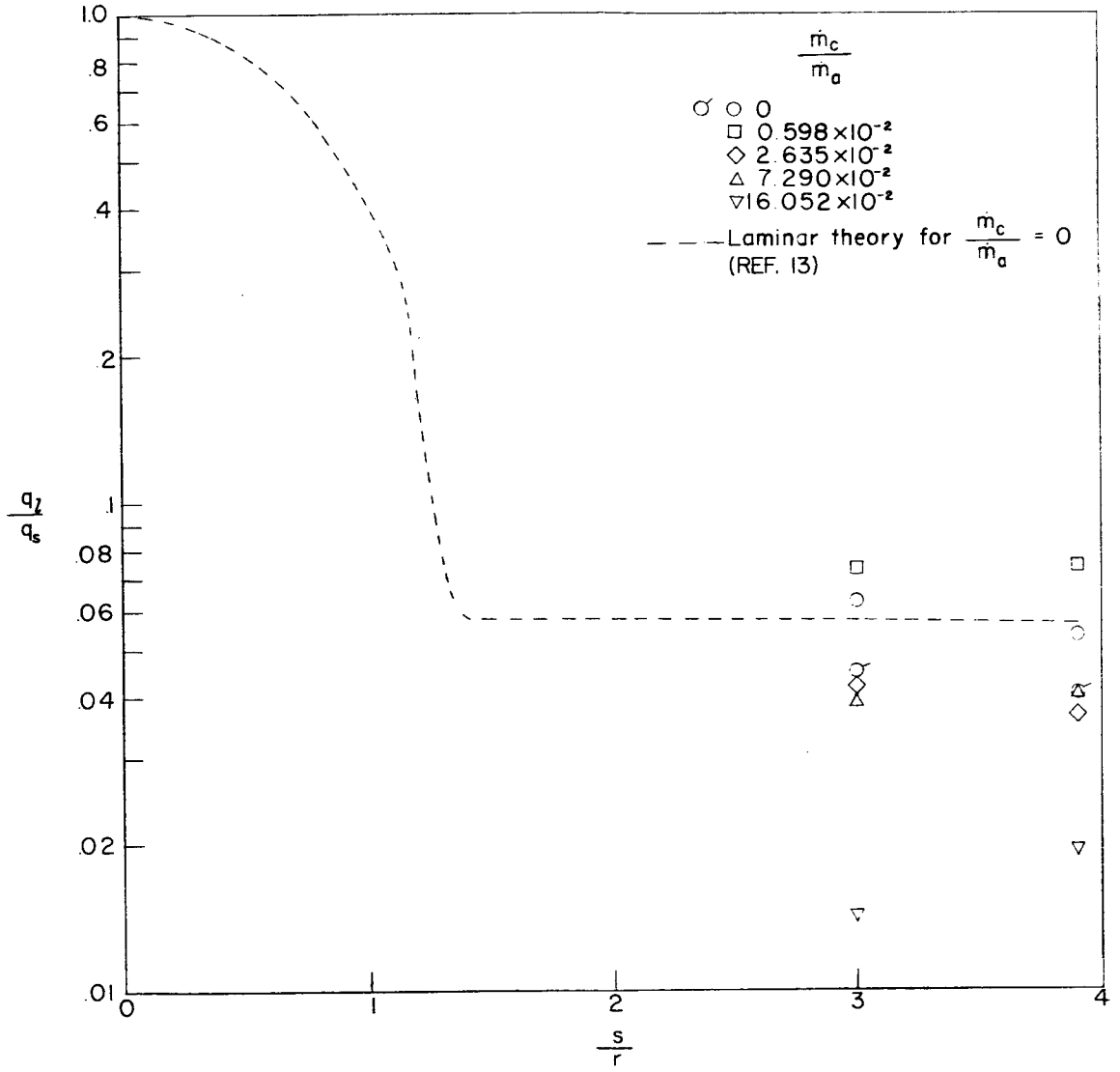

(b) Nitrogen coolant.

Figure 7.- Continued.

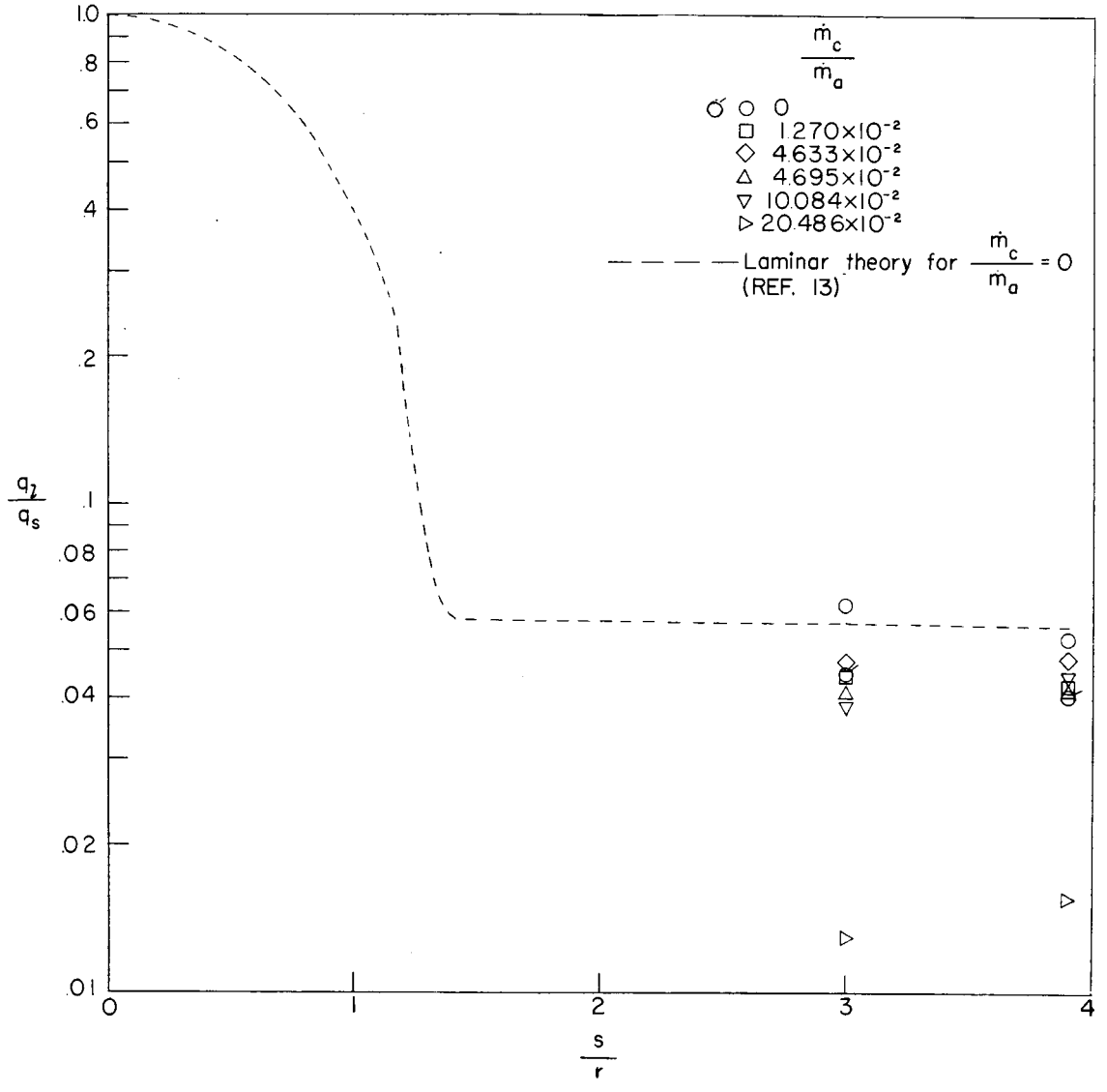

(c) Argon coolant.

Figure 7.- Concluded.

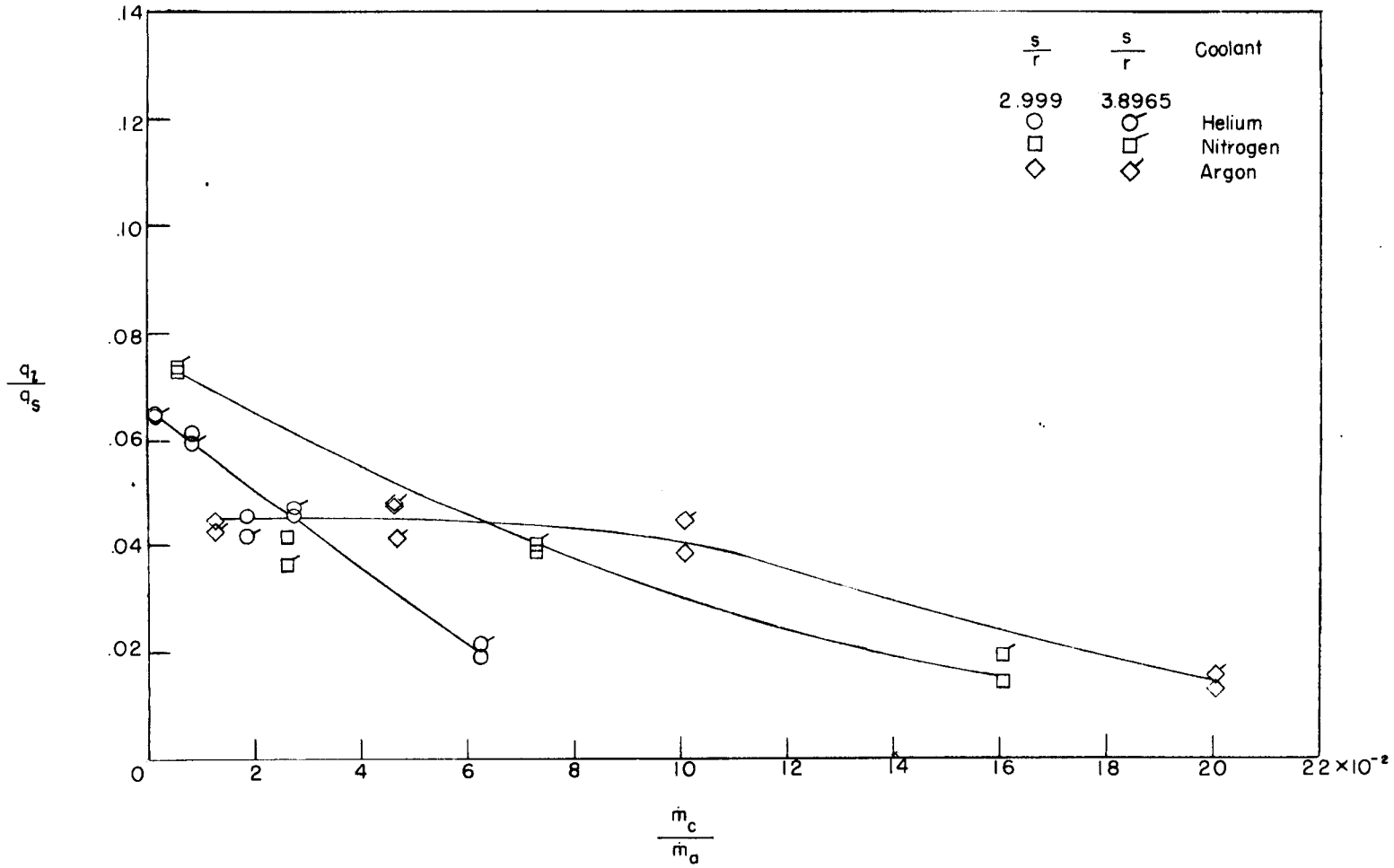

Figure 8.- Heat transfer as a function of mass injection.

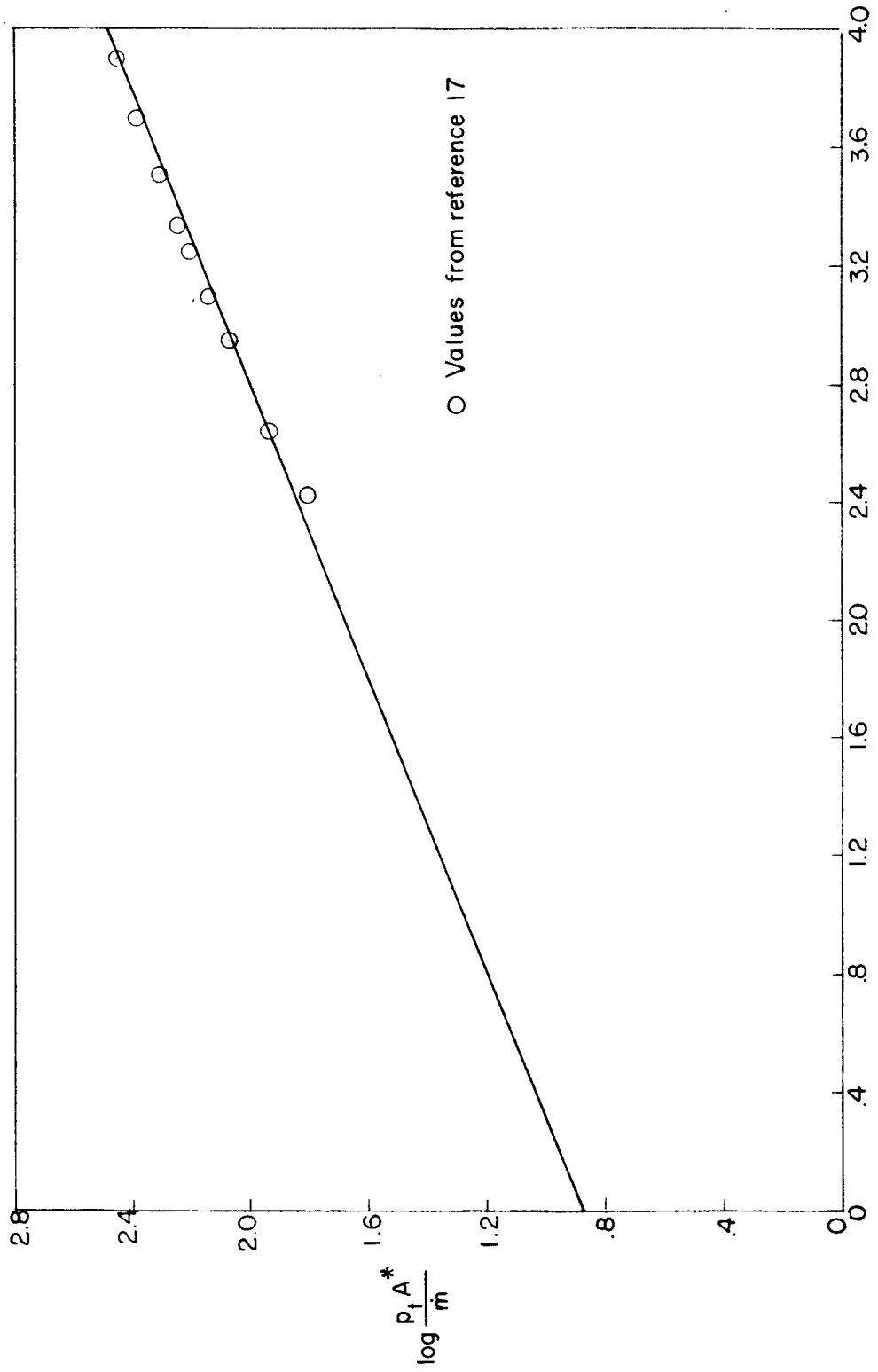

Figure 9.- Enthalpy variation with mass flow and stagnation pressure.